

Through-focus Scanning Optical Microscopy Applications

Ravi Kiran Attota*

Engineering Physics Division, National Institute of Standards and Technology
Gaithersburg, MD 20899, USA

ABSTRACT

We present a partial application space of the metrology method referred to as through-focus scanning optical microscopy (TSOM), with most number of favorable attributes as a metrology and process control tool. TSOM is a NIST-developed, high-throughput and low-cost optical metrology tool for dimensional characterization with sub-nanometer measurement resolution of nano-scale to microscale targets using conventional optical microscopes, with many unique benefits and advantages. In TSOM the complete set of out-of-focus images are acquired using a conventional optical microscope and used for dimensional analysis. One of the unique characteristics of the TSOM method is its ability to reduce or eliminate optical cross correlations, often challenging for optical based metrology tools. TSOM usually has the ability to separate different dimensional differences (i.e., the ability to distinguish, for example, linewidth difference from line height difference) and hence it is expected to reduce measurement uncertainty.

TSOM is applicable to a wide variety of target materials ranging from transparent to opaque, and shapes ranging from simple nanoparticles to complex semiconductor memory structures, including buried structures under transparent films. TSOM has been successfully applied to targets ranging from one nm to over 100 μm (over five orders or magnitude size range). Demonstrated applications of TSOM include critical dimension (linewidth), overlay, patterned defect detection and analysis, FinFETs, nanoparticles, photo-mask linewidth, thin-film (less than 0.5 nm to 10 nm) thickness, through-silicon vias (TSVs), high-aspect-ratio (HAR) targets and others with several potential three-dimensional shape process monitoring applications such as MEMS/NEMS devices, micro/nanofluidic channels, flexible electronics, self-assembled nanostructures, and waveguides. Numerous industries could benefit from the TSOM method —such as the semiconductor industry, MEMS, NEMS, biotechnology, nanomanufacturing, nanometrology, data storage, and photonics.

Keywords: TSOM, through focus, optical microscope, nanometrology, process control, nanomanufacturing, nanoparticles, overlay metrology, critical dimension, defect analysis, dimensional analysis, MEMS, NEMS, photonics

1. INTRODUCTION

As the applications of nanotechnology and micro-technology become widespread, three-dimensional (3-D) shape analysis of microscale to nanoscale structures with sub-nanometer measurement resolution become important. Several tools and methods are available for such a metrology with their unique advantages and disadvantages. However, it is a challenge to find a universally applicable measurement tool. But an economical, versatile and high-throughput tool that provides 3-D shape measurement with least number of negatives is highly desirable, especially for industrial nanomanufacturing. Here we present some of the applications of the metrology method referred to as through-focus scanning optical microscopy (TSOM), with most number of favorable attributes as a metrology and process control tool [1-27].

TSOM is a NIST-developed, high-throughput and low-cost optical metrology tool for dimensional characterization with sub-nanometer measurement resolution of nano-scale to microscale targets using conventional optical microscopes, with many unique benefits and advantages. For this reason TSOM has been well recognized: given an R&D 100 award in 2010 [28], included in the International Technology Roadmap for Semiconductors (ITRS) [29, 30] and International Roadmap for Semiconductor Devices and Systems (IRDS) 2017 Edition: Metrology [31], for several applications, included in the SEMI document for 3-D S-IC structures [32], identified by SEMATECH for several applications[33].

*Ravikiran.attota@nist.gov; Phone: 1 301 975 5750

In conventional optical microscopy, out-of-focus images are ordinarily considered not particularly useful, especially for metrology applications. This is based on the generally accepted assumption that optical information from out of focus planes is either less useful or detrimental compared to information from the best focus plane. However, a complete set of out-of-focus images contains significantly more information about the target as compared to a single best-focus image. This additional information can be extracted by TSOM. A typical TSOM image is a cross-section constructed from the four-dimensional (4-D) optical data acquired using a conventional optical microscope as a target is scanned along the focus direction.

TSOM shows considerable promise in meeting the industrial requirement of high throughput and low-cost 3-D shape metrology. TSOM transforms a conventional and ubiquitous optical microscope into a powerful 3-D shape metrology tool and provides sub-nanoscale measurement resolution comparable to SEM and AFM in both lateral and vertical directions. One of the unique characteristics of the TSOM method is its ability to reduce or eliminate optical cross correlations, often challenging for optical based metrology tools. TSOM usually has the ability to separate different dimensional differences (i.e., the ability to distinguish, for example, linewidth difference from line height difference) and hence it is expected to reduce measurement uncertainty.

TSOM is applicable to a wide variety of target materials ranging from transparent to opaque, and shapes ranging from simple nanoparticles to complex semiconductor memory structures, including buried structures under transparent films.

TSOM has been successfully applied to targets ranging from one nm to over 100 μm (over five orders or magnitude size range). Demonstrated applications of TSOM include critical dimension (linewidth), overlay, patterned defect detection and analysis, FinFETs, nanoparticles, photo-mask linewidth, thin-film (less than 0.5 nm to 10 nm) thickness, through-silicon vias (TSVs), high-aspect-ratio (HAR) targets and others with several potential three-dimensional shape process monitoring applications such as MEMS/NEMS devices, micro/nanofluidic channels, flexible electronics, self-assembled nanostructures, and waveguides. Numerous industries could benefit from the TSOM method —such as the semiconductor industry, MEMS, NEMS, biotechnology, nanomanufacturing, nanometrology, data storage, and photonics. Here we highlight some examples for which TSOM was applied.

2. TSOM IMAGING METHOD

A brief introduction to the creation of TSOM image from the through-focus optical data is presented here. First, a set of through-focus images are collected by scanning the stage on which a target is placed along the axial direction (Fig. 1, left image). Stacking the set of through-focus images at their respective focus positions creates a 3-D space filled with the optical intensity data (Fig. 1, center image). A vertical cross-section through this 3-D space creates a TSOM image (Fig. 1, right image). In the TSOM image, the X and Y axes represent distance, and focus position, respectively.

A differential TSOM (D-TSOM) image is a pixel-by-pixel difference between two normalized and aligned TSOM images [12]. If the two TSOM images are obtained using two targets with slightly different dimensions, then the D-TSOM image color pattern highlights the type of dimensional difference between the two targets [3, 9, 12]. If the two TSOM images are obtained using the same target (similar to repeated collection), then the D-TSOM image highlights noise [9, 15, 16], including optical and vibrational noise.

One way to quantify optical content of a D-TSOM (or a TSOM) image is with an optical intensity range (OIR) metric which is defined as the absolute difference between the maximum and the minimum optical intensity in a given D-TSOM (or a normalized TSOM) image and multiplied by 100 [12]. OIR represents the magnitude of the optical intensity difference. A second way is by evaluating the mean absolute value (MAV), calculated as:

$$MAV = \frac{1}{n} \sum_{k=1}^n |D-TSOM|_k$$

where N is the number of pixels in the D-TSOM image. MAV represents total optical content in a D-TSOM (or a TSOM) image. In the current work all MAVs presented are multiplied by 1000.

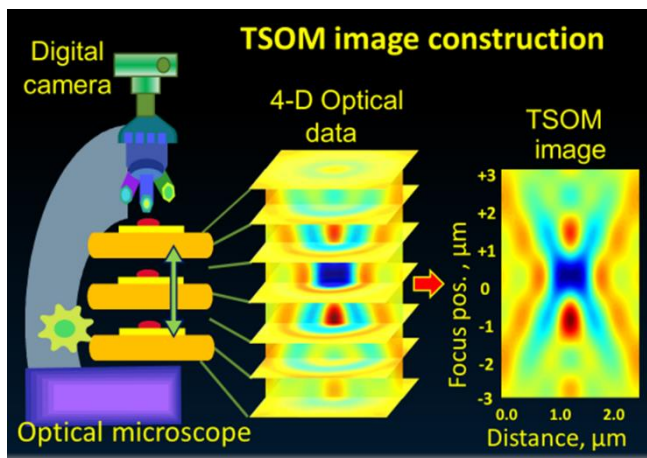


Figure 1. Video depicting a typical TSOM image construction process. <http://dx.doi.org/doi.number.goes.here>

3. APPLICATIONS OF TSOM

3.1 Defect inspection of EUV masks

The defect density of extreme ultraviolet (EUV) masks has been one of the top concerns in EUV lithography[10]. To reduce the defect level of EUV masks, defect sources must be mitigated or eliminated at each step of the mask manufacturing process. Defects on EUV masks are categorized as phase defects and amplitude defects based on the phase change or amplitude change of reflected EUV light. Amplitude defects are located on top or near the top of the multilayer structure. Phase defects are generally formed by the multilayer deposition over substrate defects (particles or pits) or are particles added during multilayer deposition.

TSOM demonstrated potential capability of detecting defects on EUV masks down to 15 nm size, and it may be able to determine depth location, with information on amplitude and phase change of light. Figure 2(a) is a simulation, using optical imaging modeling software, of applying the TSOM method to detect a bump-type phase defect having 21 nm spherical-equivalent volume diameter (SEVD). Simulations indicate that the TSOM method should have sufficient signal strength over experimental noise to detect phase defects down to 15 nm SEVD using 193 nm wavelength light. A pit type of defect exhibits distinct color reversal in comparison to the bump type of defect as shown in Fig. 2(b), clearly distinguishing the two.

Nondestructively detecting the depth of buried defects (pits or particles) in a multilayer EUV stack is a challenging task, but the simulated TSOM images for such buried particle defects do show sensitivity to the depth of particles. This suggests the possibility of inferring the depth of defects in multilayers, which is essential information for defect repair schemes. We are in the process of experimentally validating the simulation results by building a controlled blank EUV mask test structure having particles of known size placed at different known depths in the multilayer structure. This validation will be extremely beneficial for the defect repair process, resulting in major savings in time and cost. TSOM shows potential to (i) detect phase defects on EUV masks down to 15 nm SEVD, (ii) distinguish pits from bumps, and (iii) infer depth information of buried particles. The TSOM method is economical as it requires a low cost 193 nm optical microscope (compared to an AIT), and has high throughput. As a result, the TSOM method appears to be a good candidate method for detection of defects on EUV lithography masks. For more information refer to [10].

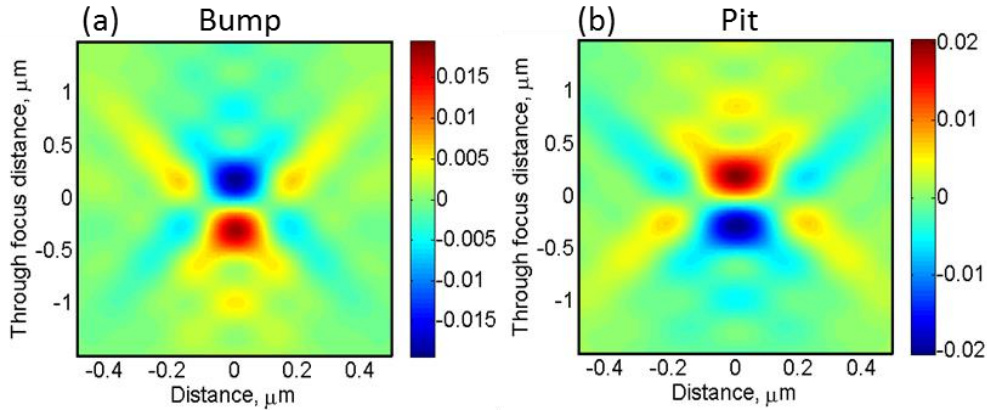


Figure 2. Simulated TSOM images of (a) bump type and (b) pit type 21 nm SEVD phase defects showing color reversal. $\lambda = 193$ nm.

3.2 Nanoparticle size determination

There is a great interest in using nanoparticles [13, 34, 35] because of their variety of biological applications. Size of the nanoparticles is a critical factor for their effective biological application. Although there are several tools available for size determination of nanoparticles, there is a concern that most of the available high-throughput methods have insufficient level of accuracy as per the definition of particle size distribution by the National Institute of Standards and Technology. In addition, there is also a concern that “soft” or “fuzzy” nanoparticles are difficult to characterize using high-resolution methods such as transmission electron microscopy (TEM) or scanning electron microscopy (SEM), since these methods

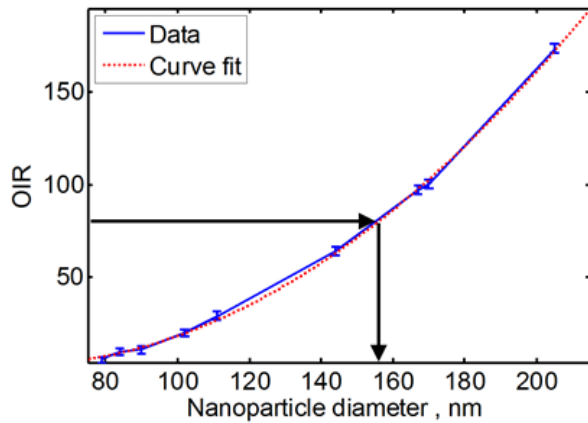


Figure 3. Calibration curve generated using the measured TSOM images of spherical Au nanoparticles on a Si substrate. Arrow marks indicate size determination of an “unknown” spherical Au nanoparticle using the OIR value of the TSOM image. Wavelength = 520 nm, $\sigma = 0.176$ (Illumination NA = 0.15, collection NA = 0.85).

deform nanoparticles during the measurement process. The most widely used dynamic light scattering (DLS) method also has several limitations such as systematic offset compared with TEM measurements.

Applicability of TSOM was tested for spherical Au nanoparticles. Using an SEM, spherical-shaped Au nanoparticles spread on a Si substrate were identified and their sizes were measured. The identified Au nanoparticles were then analyzed using the TSOM method. OIR values from the TSOM images were plotted as a function of the SEM-measured mean particle diameters. A fitted curve using these values results in a calibration curve (or library) as shown in Fig. 3 for the Au nanoparticles under the experimental conditions used. The 156 nm diameter nanoparticle was considered as a test target and hence its value was not included in the calibration curve. The size of the test target was measured by comparing its OIR value with the calibration curve. As shown in Fig. 3, the TSOM-measured diameter is 153 nm, while the SEM-measured diameter is 156 nm. For more information refer to [13].

3.3 Determine the number of nanoparticles in a cluster

There are a few optical microscopy techniques to identify the number of the nanoparticles by measuring the optical

properties of the nanoparticles such as the fluorescence lifetime, spectrum, and time-dependent intermittence [36]. However, all these optical microscopy techniques are restricted to the fluorescent nanomaterials. High-resolution imaging tools such as scanning electron microscope (SEM), transmission electron microscope, and atomic force microscope are capable of counting the number of the nanoparticles in a cluster. However, they do not have the functionality to measure photophysical properties. Most photophysical properties of the nanoparticles are measured with optical microscopes [37]. Therefore, adding the functionality to determine the number of nanoparticles by the optical microscope gives a significant advantage to users and also helps them quantitatively interpret the photophysical properties of the nanoparticle clusters.

After spreading 93 nm mean size polystyrene nanoparticles onto a Si substrate, monomers, dimers, trimers, and tetramers were identified using SEM. The same clusters were analyzed using TSOM and their OIR values were plotted as shown in Fig. 4. We can observe that the optical content (OIR) of the TSOM images increased with the number of the particles in the clusters. To confirm the validity of the trends observed from the measurements, we also simulated optical TSOM images under the exact experimental conditions. These results are also plotted in Fig. 4. Even though there are some differences between the measurements and the simulations, the overall trend matches very well as a function of the number of particles in the clusters and thus provides confidence in the process. For more information refer to [14].

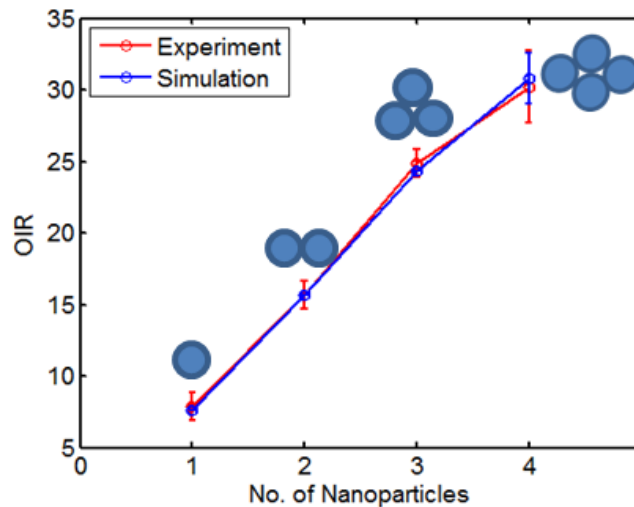


Figure 4. A plot of the OIR values from the measurements and the simulations for the different clusters of polystyrene nanoparticles

3.4 Resolving three-dimensional shape of sub-50 nm wide lines

The ability to meaningfully resolve (or distinguish) three-dimensional (3-D) shape and variations at the nanometer scale is extremely beneficial in the current world of nanotechnology. There is a significant need for tools with the ability to resolve objects at the nanometer scale while also being economical, versatile, robust, easy-to-use, non-destructive, non-contaminating, and non-contact, yet capable of high throughput. It is additionally beneficial if the tool has the ability to resolve feature shape in 3-D. We experimentally demonstrate that the three-dimensional (3-D) shape variations of nanometer-scale objects can be resolved and measured with sub-nanometer scale sensitivity using conventional optical microscopes by analyzing 3-D optical data using TSOM.

The results show that TSOM-determined cross-sectional (3-D) shape differences of 30 nm to 40 nm wide lines agree well with critical-dimension atomic force microscope measurements (Fig. 5). The TSOM method showed a linewidth uncertainty of 1.22 nm ($k=2$). Complex optical simulations are not needed for analysis using the TSOM method, making the process simple. For more information refer to [12].

Simulations demonstrate the potential usefulness of TSOM for 3-D shape metrology of fin structures for the 22 nm and 16 nm nodes. TSOM shows the ability to detect sub-nanometer, three-dimensional shape variations such as line height, sidewall angle, width, and pitch in fins of fin-shaped field effect transistor structures using conventional optical microscopes. Sensitivity to various perturbations appears sufficient and distinct (Table. 1). In addition to economical metrology hardware, the substantially smaller area targets needed result in further potential cost savings. If paired with CD-SEM, scatterometry (optical critical dimension) or other widely-used tools, an inexpensive tool such as TSOM could be a key component of a good hybrid metrology solution. For more information refer to [9].

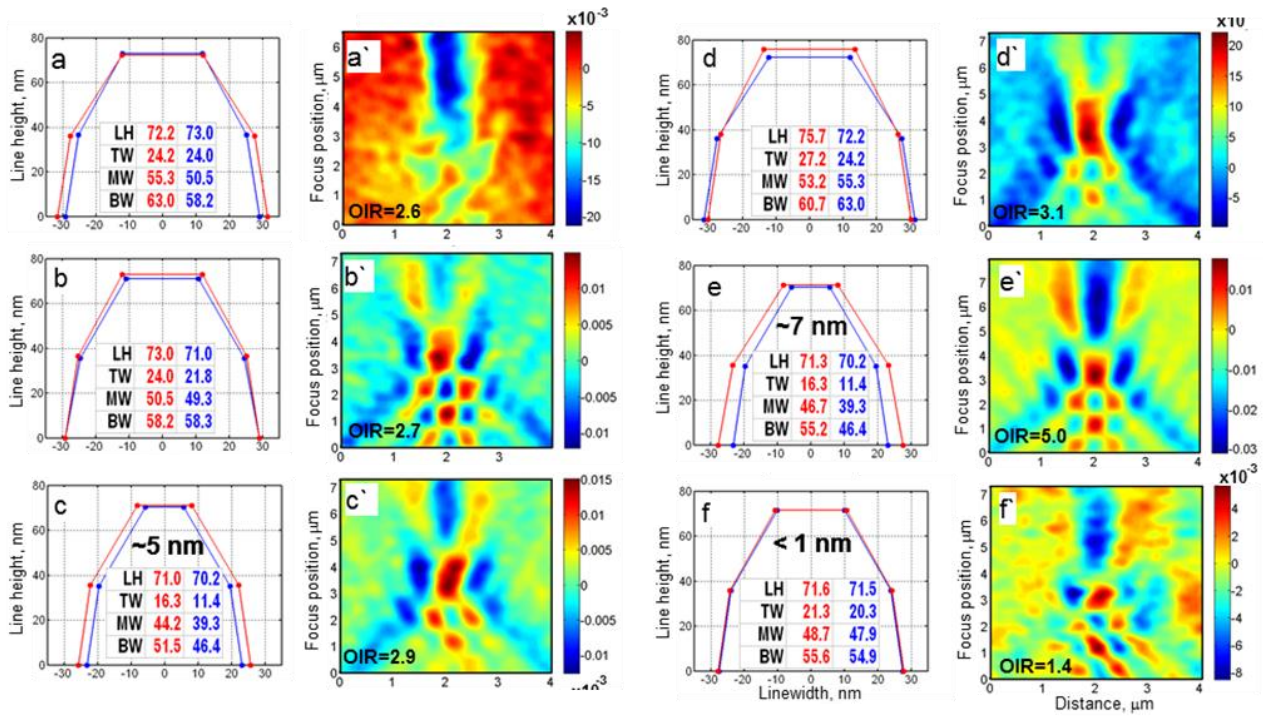


Figure 5. Experimental results for size and shape analysis of isolated lines. (a,b,c,d,e,f) Plots showing the CD-AFM-measured dimensions of the pair of lines selected for TSOM analysis. Solid dots indicate the locations of the CD-AFM measured values. Line height (LH), top width (TW), middle width (MW) and bottom width (BW, in nanometers) are shown in order for the pair of lines. (a',b',c',d',e',f') are the corresponding DTIs along with their OIR values for the selected pairs of lines. Different types of shape changes (a,b,c,d,) produced DTIs with distinctly different patterns (a',b',c',d'). Varying magnitudes of the same shape difference as indicated in c,e,f produced similarly patterned DTIs (c',e',f'). The OIR of the DTI signal, shown by the color bar scale, is greater for larger differences in the linewidth values.

ITRS Node	λ	LW (CD)	SWA	Box recess	LH	PW	High K thickness
nm	nm	nm	Degree	nm	nm	nm	nm
22	546	0.04	0.06	0.28	0.08	0.44	?
22	248	0.21	0.38	<u>≥ 3</u>	0.15	1.11	?
22	193	0.08	0.1	<u>≥ 2</u>	0.04	0.2	0.05
16	546	0.07	0.26	<u>≥ 3</u>	0.24	0.14	?
16	258	0.12	0.45	<u>≥ 3</u>	0.2	0.41	?
16	193	0.13	0.27	<u>≥ 3</u>	0.15	0.89	?

Table 1. Summary of results of varying features at a given ITRS node and TSOM wavelength. The value of the smallest perturbation that can be detected over noise is given in the table. Underline = no sensitivity, Italics = a high likelihood of cross-correlation; Normal = better sensitivity, and Bold = the best sensitivity.

3.5 Optical microscope illumination analysis

Illumination distortion in an optical microscope can lead to quantitative misinterpretation of measurements that are based on through-focus images, such as confocal microscopy [38], 3-D super-resolution imaging of nanoparticles [39], optical nanoparticle and bacteria tracking methods [40-44], and the TSOM method [2, 21, 27]. Similar to TSOM, the optical tracking methods also use a low illumination NA [39, 44], making the current study even more relevant to them also. We speculate that the slanted TSOM image reported in [21] could be due to distorted illumination, probably caused by illumination aperture misalignment. Hence, it is advisable to measure and correct the distortions in the illumination to make a proper analysis for these methods.

Distortions in illumination can be investigated by evaluating the angular illumination asymmetry (ANILAS) maps [45, 46]. Here we show that such aberrations in the illumination also produce distorted TSOM images, namely lateral image shift with focus height. We demonstrate here that the slant in TSOM images caused by illumination aberrations of this type can nearly be eliminated by simply re-aligning the aperture diaphragm to the optical axis. Conversely, the slanted TSOM images could provide an alternative, more convenient way of measuring ANILAS.

For example, illumination distortions at the sample plane of an optical microscope can be artificially created by moving the aperture diaphragm along the optical axis as shown in Figs. 6(a1) and 6(b1). This results in illumination distortions as shown by ANILAS maps in Figs. 6(a2) and 6(b2). There is a good correlation between the ANILAS map and the slant in the TSOM image. The TSOM image at the center of the ANILAS map (lowest asymmetry) is upright (Fig. 6(ab4)), indicating that no matter where the “sweet spot” is located in the FOV, the through-focus data at that location provides a more undistorted result. This also shows the importance of determining the location of the “sweet spot” in the FOV. For such an asymmetric illumination condition, the TSOM image of a vertical line is slanted despite being at the center of the FOV (Fig. 6(b4)), similar to the illumination condition in Fig. 6(a4). However, the type of slant in the TSOM image (either left or right) depends on the location of the line target with respect to the center ANILAS region. The slant in the TSOM images are toward the left and the right, for the line targets located on the left and on the right sides of the center of the lowest-ANILAS region, respectively. Hence by observing and analyzing the slant in a TSOM image, illumination distortions can be determined. For more information refer to [19].

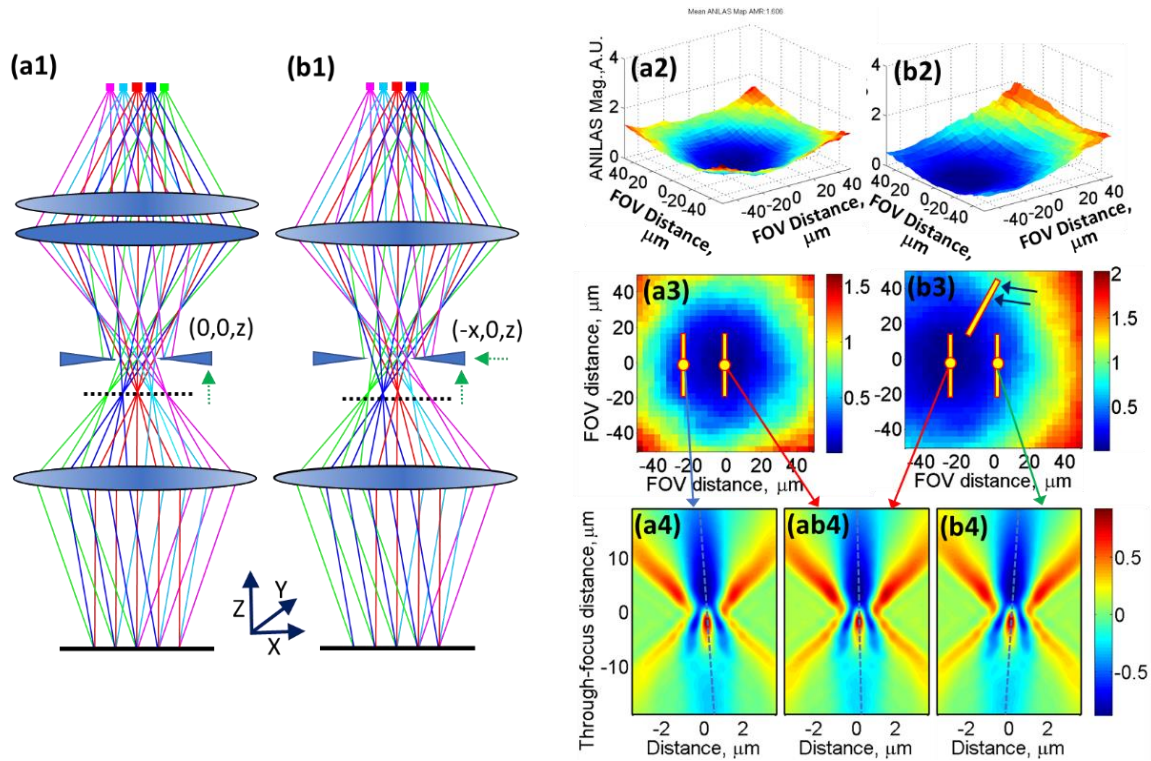


Figure 6. Schematics showing angular illuminations at the sample plane with the aperture diaphragm moved along the optical axis toward the field diaphragm for (a1) no lateral shift ($X = 0, Y = 0, Z = z$), and (b1) with finite lateral (left) shift in the X direction ($X = -x, Y = 0, Z = z$). (a2) (a3) and (a4) are the 3-D ANILAS map, 2D ANILAS map and TSOM image, respectively, for the illumination condition shown in (a1) with no lateral shift ($X = 0, Y = 0, Z = (1250 \pm 5) \mu\text{m}$). (a4) was obtained by placing the line at the location and in the orientation as shown by the arrow mark in (a3). (b2), (b3) and (b4) are the 3-D ANILAS map, 2D ANILAS map and TSOM image, respectively, for the illumination condition shown in (b1) with $(20 \pm 2) \mu\text{m}$ lateral left shift ($X = (-20 \pm 2) \mu\text{m}, Y = 0, Z = (1250 \pm 5) \mu\text{m}$). (b4) was obtained by placing the line vertically at the location as shown by the arrow mark in (b3). (ab4) represents a typical upright TSOM image obtained by placing the vertically oriented line at the locations as indicated in (a3) and (b3) by red arrow marks. All the TSOM images were obtained using a 950 nm wide line.

3.6 Overlay Analysis

An overlay target was designed for double patterning. Using both simulations and experimental measurements, the TSOM method demonstrated the potential for near 0.1-nm measurement resolution. The design consists of line gratings with alternate lines formed during two process steps. The complete overlay target consists of at least five adjacent gratings with five designed overlay offsets as shown in Fig. 7(a). A simulated TSOM image of such an overlay target is shown in Fig. 7(b) for zero process overlay. Optical contrast of the TSOM image increases with a greater overlay offset. The TSOM image changes as shown in Fig. 7(c) for a 2 nm process overlay offset. Optical intensities can be integrated in each designed overlay section of the target and plotted as a function of the designed overlay offset as shown in Fig. 7(d). In these plots, the minimum point indicates the process overlay offset.

Overlay targets were fabricated based on the composite overlay design. A typical optical image of one such experimental composite overlay target is shown in Fig. 7(e) for zero process overlay, showing very little signal. The measured TSOM image using such a target is shown in Fig. 7(f). As expected, optical contrast increases with greater overlay and validates the simulation results. The composite overlay targets are self-calibrating, robust to process variations and optical

aberrations, and highly sensitive, potentially providing near 0.1-nm overlay measurement resolution for double or multiple patterned process applications. TSOM-based analysis for other types of overlay targets can be found in Ref. [47].

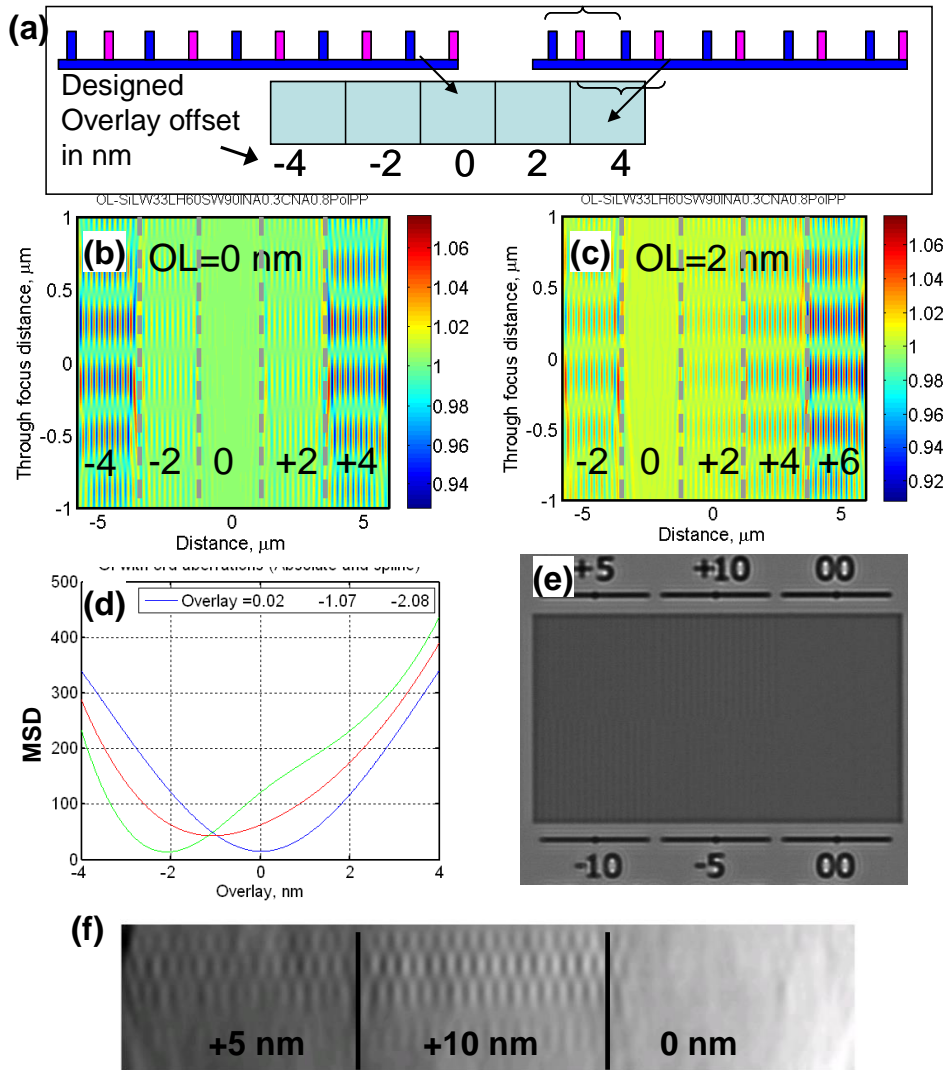


Figure 7. (a) Composite overlay target design composed of multiple designed overlay offsets as indicated for double patterning. Simulated TSOM images of the composite overlay target for (b) zero and (c) 2 nanometer overlay offsets showing increased image contrast with increased overlay offsets ($\lambda = 193 \text{ nm}$). (d) A plot of integrated optical intensities (MSD) as a function of overlay offset (from simulations). Experimentally acquired (e) optical image and (f) TSOM image of a composite overlay target using $\lambda = 546 \text{ nm}$ (designed overlay offsets shown are in nm).

3.7 Dimensional Analysis of Through-Silicon Vias (TSVs)

TSVs require truly 3-D metrology tools for dimensional analysis as they extend as deep as $50 \mu\text{m}$ with diameters as large as $5 \mu\text{m}$. The TSOM method is ideally suited for dimensional analysis of large targets such as TSVs. Simulated differential TSOM images for diameter and depth change are shown in Fig. 8. As expected, a change in diameter (Fig. 8(a)) results in a distinctly different signal than a change in depth (Fig. 8(b)). Based on the signal strength in these simulated differential

images, it may be possible to detect changes as small as a few nanometers in the diameter and depth of 5 μm diameter and 25 μm deep TSVs. Similar type of defect analysis could be applied to MEMS devices.

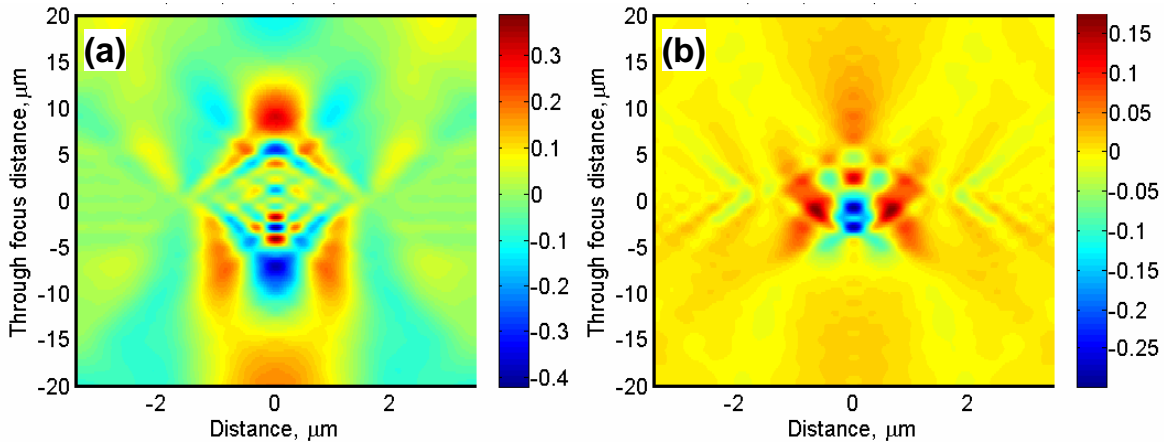


Figure 8. Simulated differential TSOM images for through-silicon vias (TSVs) (a) for 20 nm difference in the diameter, and (b) 20 nm difference in the depth of 5 μm diameter and 25 μm deep through-silicon via using $\lambda = 546 \text{ nm}$.

3.8 Patterned Defect Analysis

The main challenge facing defect inspection is the expected loss of sensitivity in conventional bright field technologies. Historically, gradual improvements to bright field have successfully extended its use to smaller nodes; however, recent theoretical work indicates that this may no longer be a useful path near the 11 nm node due to significant loss of defect signal. It is therefore necessary to explore alternative approaches that may bridge this gap from the perspective of both sensitivity and throughput. To assess the defect inspection capabilities of TSOM for sub-22 nm nodes, we first constructed a simplified gate-level layout representing conventional planar gate structures with CDs and pitches of varying dimensions. For simplicity, both the structures and the underlying substrate were modeled as Si. The simulation methodology consisted of generating TSOM images for reference targets and defect targets and subsequently obtaining a differential image by subtracting intensities pixel by pixel for each condition studied. This methodology is analogous to what is done in conventional defect inspection and allows isolating the defect signal from the background. Figure 9 and table 2 depict the simulation parameters and defect structures used in this study.

Optical Parameters	
Wavelength (nm)	546, 248
Polarization angle (degrees)	0, 90
Structural Parameters	
Gate CDs (nm)	11, 15, 20
Defect Size (nm)	5 – 15
Defect Height (nm)	8 (25%), 20 (50%), 40 (100%)
Gate Pitch (nm)	60, 90, 130

Table 2. Simulation conditions for the defect structures

Although several results are available [6] here we present an important aspect of defect inspection showing how pattern density affects defect detectability. To evaluate the effects of this parameter on defect signal intensity, we performed simulations at two different pitches, 90 nm and 60 nm, for an 11 nm gate layout. All defects were simulated at three different sizes of nominal CD: 150 %, 100 %, and 50 %. Optical illumination was simulated at 248 nm and two different polarizations, 0 and 90 degrees. Figure 10 shows an excerpt of the results from this set of simulations. Once again, the modeling shows that TSOM should be capable of detecting all defects down to the smallest size (5.5 nm). In this case, all successful detection events occurred under 90 degree polarization illumination. The smallest OIR is greater than 2, showing that this optical setup might be able to detect smaller defects, perhaps at tighter pitches. The results at 0 degree polarization show once more

that the type A defect produces the weakest signal, which is below the detectable limit of 1 % in at least one case for all pitch values studied.

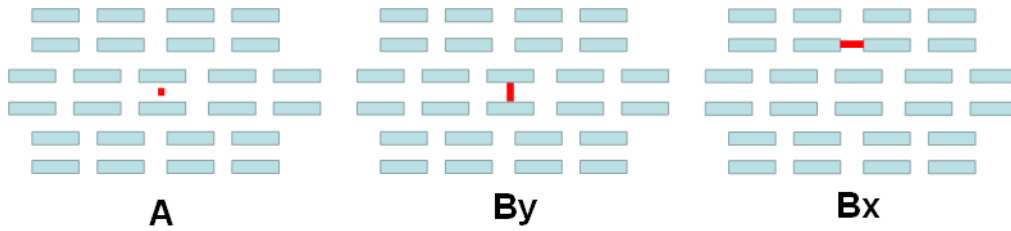
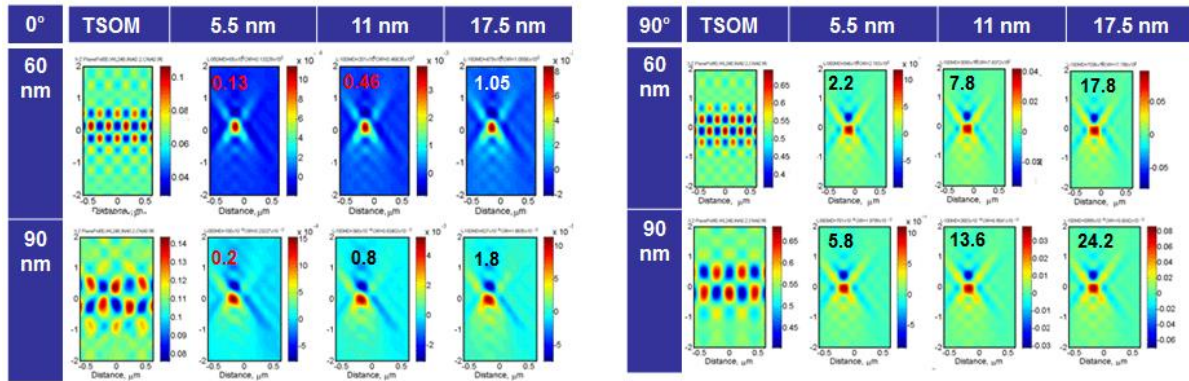


Figure 9. Summary of optical and structural parameters varied and diagrams showing the type of defects studied.



Structural Parameters	
Gate CD (nm)	11
Defect Size (nm)	5.5, 11, 17.5
Gate Pitch (nm)	60, 90
Optical Parameters	
Wavelength (nm)	248
Polarization angle (degrees)	0, 90

Figure 10. TSOM and differential TSOM images showing the effect of gate pitch on defect detectability. Images correspond to three type A defect sizes. Illumination wavelength is 248 nm, and both polarization conditions are shown. Inset numbers correspond to the OIR of the differential TSOM image. For an OIR > 1, the modeling predicts that the defect should be detectable. The table shows the set of varied parameters.

4. CONCLUSIONS

TSOM is a high-throughput and low-cost optical metrology tool for 3-D shape process monitoring and characterization. We have present several recent applications of TSOM. In addition to these we are in the process of evaluating TSOM for several other applications in diverse areas. TSOM achieved sub-nanometer measurement resolution with most number of favorable attributes as a metrology and process control tool. TSOM can be applied to sub-10 nm to over 100 μm size targets with many unique benefits and advantages. TSOM usually has the ability to separate different dimensional differences (i.e., the ability to distinguish, for example, linewidth difference from line height difference) and hence it is expected to reduce measurement uncertainty. Numerous industries could benefit from TSOM—such as the semiconductor industry, MEMS, NEMS, biotechnology, nanomanufacturing, nanometrology, data storage, and photonics.

ACKNOWLEDGEMENTS

The author would like to acknowledge the collaboration of John Kramar, Ronald Dixson, Emil Agocs, Haesung Park, Peter

Weck, Benjamin Bunday, Victor Vartanian, Heyonggon Kang, Vipin Tondare, Prem Kavuri, Andras Vladar, Rick Silver, Richard Kasica, Richard Allen, George Orji, Abraham Arceo, Vibhu Jindal, James Potzick, Michael Stocker and Lei Chen.

REFERENCES

- [1] R. Attota, R. M. Silver, and J. Potzick, "Optical illumination and critical dimension analysis using the through-focus focus metric method - art. no. 62890Q," *Novel Optical Systems Design and Optimization IX*, 6289, Q2890-Q2890 (2006).
- [2] R. Attota, T. A. Germer, and R. M. Silver, "Through-focus scanning-optical-microscope imaging method for nanoscale dimensional analysis," *Optics Letters*, 33(17), 1990-1992 (2008).
- [3] R. Attota, R. G. Dixon, J. A. Kramar *et al.*, "TSOM Method for Semiconductor Metrology," *Proc. SPIE*, 7971, 79710T (2011).
- [4] R. Attota, R. G. Dixon, and A. E. Vladar, "Through-focus Scanning Optical Microscopy," *Scanning Microscopies 2011: Advanced Microscopy Technologies for Defense, Homeland Security, Forensic, Life, Environmental, and Industrial Sciences*, 8036, (2011).
- [5] R. Attota, and R. Silver, "Nanometrology using a through-focus scanning optical microscopy method," *Measurement Science & Technology*, 22(2), (2011).
- [6] A. Arceo, B. Bunday, V. Vartanian *et al.*, "Patterned Defect & CD Metrology by TSOM Beyond the 22 nm Node," *Metrology, Inspection, and Process Control for Microlithography Xxvi*, Pts 1 and 2, 8324, (2012).
- [7] B. Damazo, R. Attota, P. Kavuri *et al.*, "Nanoparticle Size and Shape Evaluation Using the TSOM Method," *Metrology, Inspection, and Process Control for Microlithography Xxvi*, Pts 1 and 2, 8324, (2012).
- [8] A. Arceo, B. Bunday, and R. Attota, "Use of TSOM for sub-11 nm node pattern defect detection and HAR features," *Metrology, Inspection, and Process Control for Microlithography Xxvii*, 8681, (2013).
- [9] R. Attota, B. Bunday, and V. Vartanian, "Critical dimension metrology by through-focus scanning optical microscopy beyond the 22 nm node," *Applied Physics Letters*, 102(22), (2013).
- [10] R. Attota, and V. Jindal, [Inspecting mask defects with through-focus scanning optical microscopy] *SPIE Newsroom*, August 8 (2013).
- [11] V. Vartanian, R. Attota, H. Park *et al.*, "TSV reveal height and dimension metrology by the TSOM method," *Metrology, Inspection, and Process Control for Microlithography Xxvii*, 8681, (2013).
- [12] R. Attota, and R. G. Dixon, "Resolving three-dimensional shape of sub-50 nm wide lines with nanometer-scale sensitivity using conventional optical microscopes," *Applied Physics Letters*, 105(4), (2014).
- [13] R. Attota, P. P. Kavuri, H. Kang *et al.*, "Nanoparticle size determination using optical microscopes," *Applied Physics Letters*, 105(16), (2014).
- [14] H. Kang, R. Attota, V. Tondare *et al.*, "A method to determine the number of nanoparticles in a cluster using conventional optical microscopes," *Applied Physics Letters*, 107(10), (2015).
- [15] R. Attota, "Noise analysis for through-focus scanning optical microscopy," *Optics Letters*, 41(4), 745-748 (2016).
- [16] R. Attota, and J. Kramar, "Optimizing noise for defect analysis with through-focus scanning optical microscopy," *Proc. SPIE*, 9778, 977811 (2016).
- [17] R. K. Attota, and H. Kang, "Parameter optimization for through-focus scanning optical microscopy," *Optics Express*, 24(13), 14915-14924 (2016).
- [18] R. K. Attota, P. Weck, J. A. Kramar *et al.*, "Feasibility study on 3-D shape analysis of high-aspect-ratio features using through-focus scanning optical microscopy," *Optics Express*, 24(15), 16574-16585 (2016).
- [19] R. K. Attota, and H. Park, "Optical microscope illumination analysis using through-focus scanning optical microscopy," *Opt Lett*, 42(12), 2306-2309 (2017).
- [20] S.-W. Park, J. H. Lee, and H. Kim, [3D digital holographic semiconductor metrology using Fourier Modal Method] *OSA*, Fukuoka, Japan(2017).
- [21] S. Han, T. Yoshizawa, S. Zhang *et al.*, "Tip/tilt-compensated through-focus scanning optical microscopy," *Proc. of SPIE*, 10023, 100230P (2016).
- [22] M. Ryabko, A. Shchekin, S. Koptyaev *et al.*, "Through-focus scanning optical microscopy (TSOM) considering optical aberrations: practical implementation," *Optics Express*, 23(25), 32215-32221 (2015).
- [23] M. Ryabko, S. Koptyaev, A. Shcherbakov *et al.*, "Motion-free all optical inspection system for nanoscale topology control," *Optics Express*, 22(12), 14958-14963 (2014).
- [24] M. Ryabko, Koptyev, S., Shchekin, A., Medvedev, A., "Improved critical dimension inspection for the

semiconductor industry,” SPIE Newsroom, (2014).

- [25] V. Vartanian, R. Attota, H. Park *et al.*, “TSV reveal height and dimension metrology by the TSOM method,” Proc. of SPIE, 8681, 86812F (2013).
- [26] S. Usha, Shashikumar, P.V., Mohankumar, G.C., Rao, S.S., “Through Focus Optical Imaging Technique To Analyze Variations In Nano-Scale Indents,” International Journal of Engineering Research & Technology, 2(5), 18 (2013).
- [27] M. V. Ryabko, S. N. Koptyaev, A. V. Shcherbakov *et al.*, “Method for optical inspection of nanoscale objects based upon analysis of their defocused images and features of its practical implementation,” Optics Express, 21(21), 24483-24489 (2013).
- [28] M. Esser, [NIST Nanoscale Dimensioning Technique Wins R&D 100 Award], (2010).
- [29] S. I. Association, [The International Technology Roadmap for Semiconductors (ITRS)] Semiconductor Industry Association, San Jose(2016).
- [30] S. I. Association, [The International Technology Roadmap for Semiconductors (ITRS)], San Jose(2012).
- [31] IEEE, [International Roadmap for Semiconductor Devices and Systems 2017 Edition: Metrology] IEEE, (2018).
- [32] [SEMI 3D5-0613 Guide For Metrology Techniques To Be Used In Measurement Of Geometrical Parameters Of Through- Silicon Vias (TSVs) In 3DS-IC Structures] SEMI, (2013).
- [33] B. Bunday, T. A. Germer, V. Vartanian *et al.*, “Gaps Analysis for CD Metrology Beyond the 22 nm Node,” Metrology, Inspection, and Process Control for Microlithography Xxvii, 8681, (2013).
- [34] J. Panyam, and V. Labhasetwar, “Biodegradable nanoparticles for drug and gene delivery to cells and tissue,” Advanced drug delivery reviews, (2012).
- [35] R. M. Crist, J. H. Grossman, A. K. Patri *et al.*, “Common pitfalls in nanotechnology: lessons learned from NCI's Nanotechnology Characterization Laboratory,” Integrative Biology, 5(1), 66-73 (2013).
- [36] S. Wang, C. Querner, T. Dadosh *et al.*, “Collective fluorescence enhancement in nanoparticle clusters,” Nature Communications, 2, 364 (2011).
- [37] H. Kang, M. L. Clarke, S. H. D. P. Lacerda *et al.*, “Multimodal optical studies of single and clustered colloidal quantum dots for the long-term optical property evaluation of quantum dot-based molecular imaging phantoms,” Biomedical Optics Express, 3(6), 1312-1325 (2012).
- [38] M. Minsky, “Memoir on Inventing the Confocal Scanning Microscope,” Scanning, 10(4), 128-138 (1988).
- [39] P. Bon, N. Bourg, S. Lecart *et al.*, “Three-dimensional nanometre localization of nanoparticles to enhance super-resolution microscopy,” Nature Communications, 6, (2015).
- [40] S. Abrahamsson, J. J. Chen, B. Hajj *et al.*, “Fast multicolor 3D imaging using aberration-corrected multifocus microscopy,” Nature Methods, 10(1), 60-U80 (2013).
- [41] N. Chenouard, I. Smal, F. de Chaumont *et al.*, “Objective comparison of particle tracking methods,” Nature Methods, 11(3), 281-U247 (2014).
- [42] K. M. Taute, S. Gude, S. J. Tans *et al.*, “High-throughput 3D tracking of bacteria on a standard phase contrast microscope,” Nature Communications, 6, (2015).
- [43] L. Gardini, M. Capitanio, and F. S. Pavone, “3D tracking of single nanoparticles and quantum dots in living cells by out-of-focus imaging with diffraction pattern recognition,” Scientific Reports, 5, (2015).
- [44] J. M. Gineste, P. Macko, E. A. Patterson *et al.*, “Three-dimensional automated nanoparticle tracking using Mie scattering in an optical microscope,” J Microsc, 243(2), 172-8 (2011).
- [45] R. K. Attota, “Step beyond Kohler illumination analysis for far-field quantitative imaging: angular illumination asymmetry (ANILAS) maps,” Optics Express, 24(20), 22616-22627 (2016).
- [46] R. Attota, and R. Silver, “Optical microscope angular illumination analysis,” Optics Express, 20(6), 6693-6702 (2012).
- [47] R. Attota, M. Stocker, R. Silver *et al.*, "Through-focus scanning and scatterfield optical methods for advanced overlay target analysis." 7272, 13.